JOTCS A
Journal of the Turkish Chemical Society
Section: A
Chemistry
TURKISH CHEMICAL SOCIETY

Adsorption of the *Meso*-Tetra-*p*-Tolylporphyrin ($TTPH_2$) and *Meso*-Tetra-Naphthylporphyrin ($TNPH_2$) onto Montmorillonite

Jasim Hamadi Hassen[1]*, Jack Silver[2]

[1]University of Anbar, College of Pharmacy, Department of Pharmaceutical Chemistry, Ramadi, Iraq.
[2]University of Brunel, Wolfson Centre for Material Processing, London, UK.

Abstract: The behavior of two porphyrin compounds, *meso*-tetra-*p*-tolylporphyrin ($TTPH_2$) and *meso*-tetra-naphthylporphyrin ($TNPH_2$) was studied and monitored during their adsorption on cation-exchanged montmorillonite clay (MMT). When these two compounds were reacted with MMT, the visible absorption spectra showed a clear shift of 10 nm higher than that found in the acetic acid solution. This suggests that the two compounds prefer to be more planar on the clay surface and, in the case of $TTPH_2$, in the MMT interlamellar layers. The basal spacing of the MMT was increased by 4.4 Å when the $TTPH_4^{2+}$ cations entered the spacers. The metal-exchanged ion in the clay is incorporated into the porphyrin rings when the $TTPH_2$ and $TNPH_2$ molecules react with MMT saturated with the metal ion of an appropriate size to fit in the porphyrin ring, such as Cu(II). The process occurred when executed in a solvent miscible with water that allowed the penetration of the hydrated sphere of the metal ion. Metalloporphyrin complexes are formed as a result of this process. The reactions were monitored using visible absorption spectra, diffuse reflectance spectra, x-ray diffraction, infrared spectra, and electron microscopy.

Keywords: Adsorption, montmorillonite, porphyrin, $TTPH_2$, $TNPH_2$.

Submitted: December 25, 2022. Accepted: May 09, 2023.

Cite this: Hassen JH, Silver J. Adsorption of the Meso-Tetra-p-Tolylporphyrin (TTPH2) and Meso-Tetra-Naphthylporphyrin (TNPH2) onto Montmorillonite. JOTCSA. 2023;10(3):641–52.

DOI: https://doi.org/10.18596/jotcsa.1224193.

***Corresponding author. E-mail:** ph.jasimhu@uoanbar.edu.iq, Tel: 009647805845839.

1. INTRODUCTION

The interaction of porphyrins with clays has been widely studied (1-6) since the late 1970s. The adsorption of two *meso*-substituted porphyrins, TPP and TPyP, on cations exchanged clays revealed that TPP is protonated during adsorption, but TPyP behavior is water-dependent. In the presence of enough water, stable metallocomplexes such as Sn(IV)TPP can be adsorbed without demetallation. While weak complexes like Fe(III)TPP are demetallated (7). The porphyrin compounds *p*-TMPyP and *m*-TMPyP were examined for their adsorption on clay. Depending on the solution used, it was shown that the orientation of both compounds on the clay monolayer was parallel and inclined concerning the clay surface (8). By using a new technique for sample preparation, cationic porphyrin was successfully intercalated onto a transparent clay membrane. When the porphyrin penetration process was carried out with water:ethanol ratio of 1:2, high-density intercalation was accomplished (6). As discussed earlier, porphyrins and other tetrapyrrole macrocycles exhibit a variety of functional qualities. They can achieve and regulate important functions like light harvesting, electron transport, and catalytic reactions when complex with metals (9). The electron-transfer reaction that occurs after light harvesting is described in a unique energy-transfer system utilizing nonaggregated cationic porphyrins adsorbed on an anionic-type clay

surface (10). The *m*-TMPyP and *p*-TMPyP were found to be the most suitable porphyrins for a quantitative energy transfer reaction (11). The photochemical energy transfer reaction was used to investigate the adsorption of two porphyrin compounds on anionic clay. Energy transfer reactions of moderate magnitude were found. The adsorbed chemicals were found to be able to travel on the surface but not from the surface to the sheet (12). The mechanism to deter the quenching of porphyrins on the surface of the clay (used as an optimum solid surface for the transfer of photochemical energy) was investigated using a range of porphyrin derivatives (13). Hydrothermal synthesis was used to produce saponite-type clays with various cation exchange capacities, which were then reacted with tetrakis(1-methylpyridinium-4-yl)porphyrin. It was found that, depending on the charge density of the saponite, the average intermolecular distance between porphyrin molecules on the saponite surface might be adjusted (14). During the adsorption of cationic porphyrin on anionic-type clay, two processes occur: surface adsorption and intercalation (15). The production of clay-porphyrin complexes and the spectrum behavior of metalloporphyrins with divalent, trivalent, and tetravalent central metals with synthetic clay have also been investigated. The complex formation, where the clay sheets were either exfoliated or layered in an aqueous colloidal solution, resulted in a spectral shift of the porphyrin Soret band to higher wavelengths (16). The energy transfer efficiency and quenching efficiency were estimated for excited energy transfer from tetrakis(1-methylpyridinium-2-yl) porphyrin to tetrakis(1-methylpyridinium-4-yl) porphyrin on an anionic clay. It was found that when the dye loadings increased, both the energy transfer efficiency and the quenching efficiency increased (17). Ion exchange was used to intercalate the Cu(II) and Fe(III) complexes of water-soluble tetrakis(*N,N,N*-trimethylanilinium)porphyrin and tetrakis(*N*-methylpyridyl)porphyrin within the interlayers of Ca(II) MMT. Porphyrins in their free base forms were also reacted with Cu(II) and Fe(III) MMT samples. It was found that when the Cu(II) metalloporphyrins contact the acidic MMT support, they do not demetalate. On smectite supports, the Fe(III) porphyrin complexes are also stable. A stable Cu(II)porphyrin-clay complex is formed when a free base porphyrin metalates on the surface of a Cu(II)-exchanged clay (18). It has been found that vanadyl and nickel *meso*-tetraphenylporphyrin are stable toward demetallation, whereas magnesium porphyrin is notably unstable (19). Adsorption studies of Sn(IV)TPyP on sodium hectorite showed that the complex demetallates to the dication TPyP when the clay is dehydrated, and it was found that the procedure is reversible (20). MMT was found to be useful to support the porphyrin complex ions $MnTPyP^+$ on the surface by adsorption (21). Moreover, the $MnTPYP^+$ ions can penetrate through the clay layers and, by ionic exchange, replace the exchangeable cations (22). Another study reported that when $MnTPyP^+$ ion has been reacted with MMT, the ion was able to intercalate in a horizontal, diagonal, and perpendicular direction (23). The porphyrin complexes $Sn(IV)TPPCl_2$, $Sn(IV)TNPCl_2$, Fe(III)TPPCl, Fe(III)TNPCl, $[(Fe(III)TPP)_2O]$, and $[(Fe(III)TNP)_2O]$, were all found to be stable on the MMT surface and show no demetallation (24).

The aim of the current research was to study the interactions that take place when two different porphyrins are adsorbed on cation-exchanged MMT clay. Moreover, knowing the new properties of these compounds and complexes when they are present on the MMT surface or between its layers, as this system has many industrial applications. The porphyrins are *meso*-tetra-tolylporphyrin ($TTPH_2$) and *meso*-tetra-napthylporphyrin ($TNPH_2$).

2. MATERIALS AND METHODS

The $TTPH_2$ and $TNPH_2$ compounds were prepared according to the methods described in the literature (25) for $TPPH_2$. The MMT sample was obtained from Podmore and Sons Ltd., England, UK. All other solvents were grade reagents and used without further purification. Diffuse reflectance spectra were recorded on a Unicam SP 700 spectrophotometer. Visible absorption spectra were recorded on Perkin-Elmer Lambda 5 UV/VIS and Beckman Du-7 spectrophotometer. Transmission electron micrographs were obtained on a JEOL 200CX transmission electron microscope at 100 KV. An ultramicrotomic technique was used to prepare the sections, on a Sorvall Porter-Blum MT2 ultramicrotome. Infrared spectra were recorded on a Perkin Elmer 1330 infrared spectrophotometer. X-ray diffraction patterns were recorded on a Philips diffractometer using CuKα radiation.

2.1. Cation-exchanged MMT Preparation

Cation-exchanged MMT samples were prepared by mixing the MMT sample with a 1 M solution of different metal chloride salts on a magnetic stirrer for 24 hours in distilled water. Then the samples were filtered and rinsed with distilled water many times until the $AgNO_3$ test for chloride ions came out negative. The samples were then dried in the air for 24 hours before being crushed into a fine powder.

2.2. Adsorption onto MMT

1 g of the cation-exchanged MMT has added to solutions of 10, 20, and 30 mg of the porphyrin compound in chloroform or acetone. The slurries were stirred for 24 hours at room temperature, then filtered, washed several times with the solvent used, and air-dried.

3. RESULTS AND DISCUSSION

3.1. Characterization of the MMT Sample

The MMT clay sample used for this study has the chemical composition presented in Table 1. The main oxides in the sample are aluminum oxide and silicon oxide, which represent 76.6% of the total composition. The rest of the oxides in the sample are of iron, titanium, calcium, sodium, and potassium.

Table 1: The chemical composition of the MMT sample.

Fe_2O_3 (%)	Al_2O_3 (%)	SiO_2 (%)	TiO_2 (%)	CaO (%)	MgO (%)	Na_2O (%)	K_2O (%)	Loss on ignition (%)	Total (%)
3.5	19.1	57.5	0.2	1.2	2.4	1.7	0.3	13.9	99.8

A limited number of impurities, including quartz, feldspar, and mica, were found in the MMT sample, as determined by X-ray diffraction studies. Figure 1 shows the X-ray diffraction pattern of the sample which showed a basal spacing of 13 Å. Since the thickness and regularity of the water layers vary depending on the exchangeable cation present as well as the conditions under which the sample was prepared, the basal spacing varies from one MMT sample to another (26).

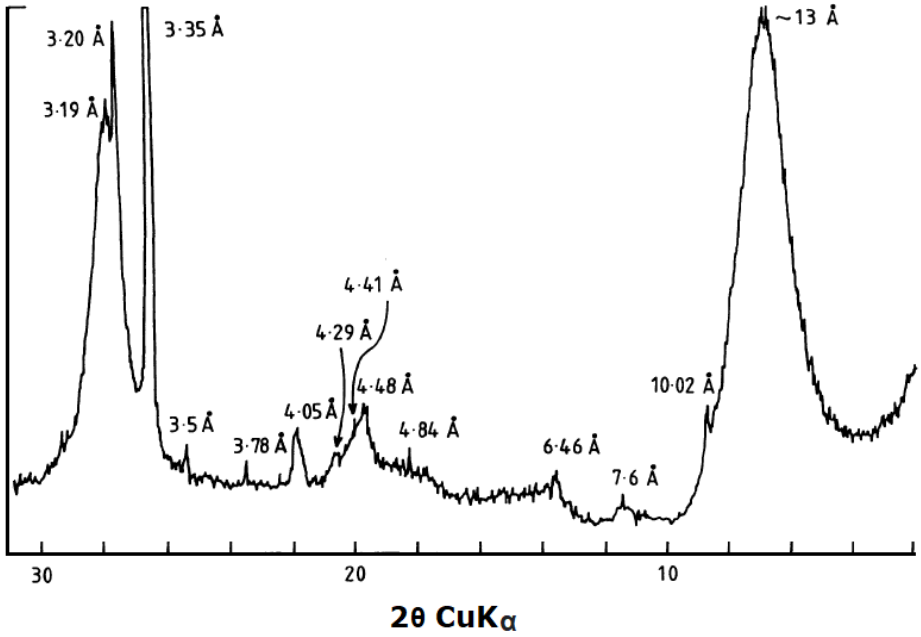

Figure 1: X-ray diffraction pattern of the MMT sample.

Characterization of the sample by IR spectra indicated the presence of Si-O stretching and OH bending, they are the primary characteristics of the MMT in the IR region. The bands have been assigned to Fe^{3+}-OH-Fe^{3+}, Al-OH-Mg, Fe^{3+}-OH-Al, Al-OH-Al, and Si-O at 800, 850, 880, 917, and 1040 cm^{-1}, respectively (27, 28).

3.2. Visible absorption and diffuse reflectance spectra

The visible spectra presented in this work are in Figures 2, 3, 5, and 7, and the diffuse reflectance spectra are shown in Figures 4 and 6. Figure 1 shows the visible absorption spectrum of the free base form of $TTPH_2$, which is identical to the spectra of $TNPH_2$. Only the intensities of the bands are different. They have a strong absorption Soret band at about 420 nm and four additional bands in the 450-700 nm range.

In acetic acid, the protonation of the free base of $TTPH_2$ causes the Soret band to be shifted to a higher wavelength, 441 nm, (Figure 3), due to the formation of the dicationic form $TTPH_4^{+2}$, while $TNPH_2$ shows a resistance toward protonation

(Figure 5). The visible spectrum of $TNPH_2$ in acetic acid indicates a significant proportion of the molecules are still present as $TNPH_2$ with little or no movement in the main Soret band. However, the presence of a smaller band (at a higher wavelength) on the right of the Soret band possibly indicates a very small amount of a dication form is present.

When the free base compounds are adsorbed onto metal cation-exchanged MMT, such as Fe(III) MMT, the spectrum of the $TTPH_2$ compound is similar to that of the dicationic form $TTPH_4^{2+}$ in shape but the position of the bands differ (Figure 3). The Soret band at 417 nm (in the unprotonated state) is shifted to 452 nm in the adsorbed state, and a broad band appears in the red region at 676 nm with a shoulder at 620 nm (Figure 3).The band at 676 nm is 10 nm higher in wavelength than that of the dication in solution.

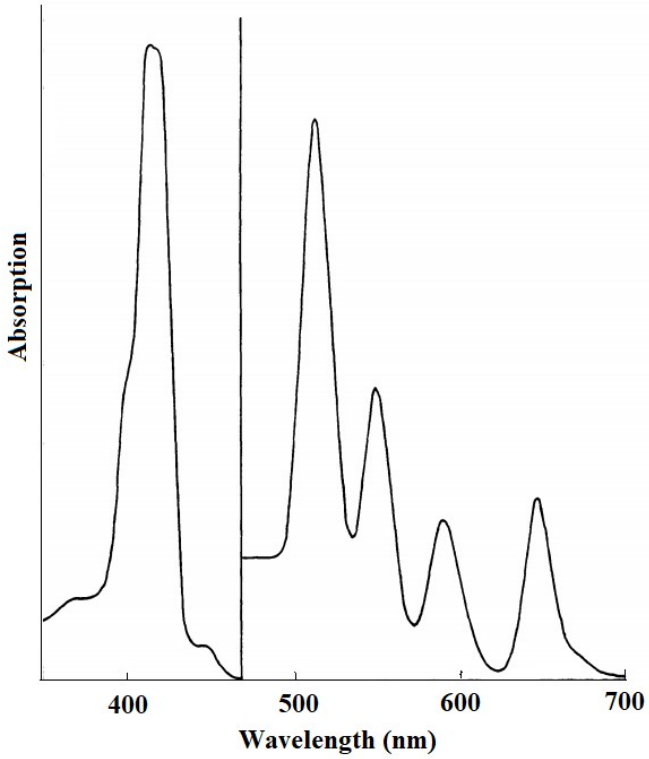

Figure 2: Visible absorption spectrum of $TTPH_2$ in chloroform. For clarity, the y-axis in the region from 470 nm to 700 nm has been magnified by 10 times.

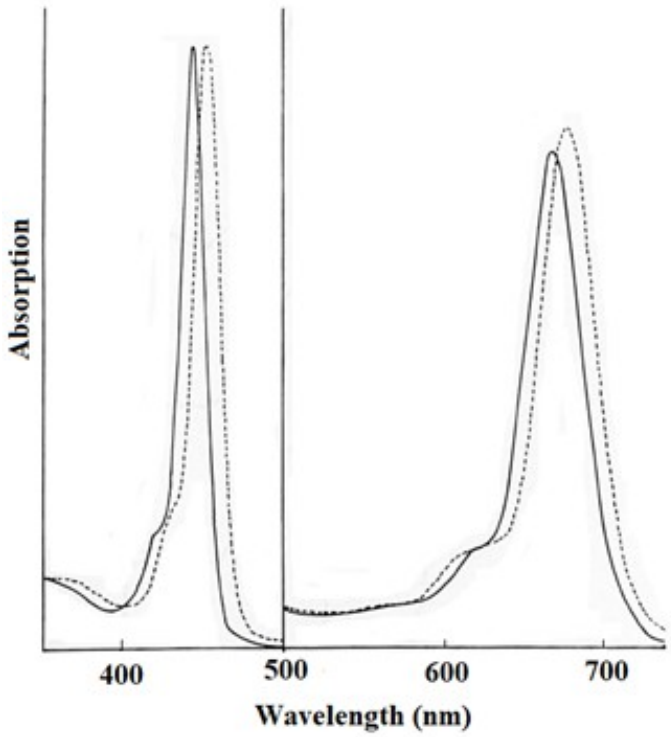

Figure 3: Visible absorption spectra of (_____) $TTPH_4^{2+}$ in glacial acetic acid, (------) $TTPH_4^{2+}$ on Fe(III) MMT after adsorption of $TTPH_2$. For clarity, the y-axis in the region from 500 nm to 700 nm has been magnified by 10 times.

The fact that the visible absorption spectrum of the adsorbed cationic form shows a clear shift of 10 nm higher than that of the cationic form found in acetic acid is evidence that the $TTPH_2$ prefers to be more planar in the MMT interlamellar and on the surface. The width of the Soret band of $TTPH_2$ on Fe(III) MMT (Figure 3) does not appear to be different to that in acid solution, implying that there is only one form of porphyrin present on the clay. The porphyrin would be expected to be restricted to a more planar conformation in the interlayer region. Clearly, some of the $TTPH_2$ must be on the clay surface as well as in the interlamellar spacing. The molecules on the surface also contribute to the absorption spectra, therefore also generating the same shift in the Soret band. The molecules can only be in contact with one surface and held flat by van der Waals forces and hydrogen bonding from the acidic surface of the MMT via surface protons. It is therefore also likely that even the porphyrin molecules in the interlayers are held flat via similar bonding rather than squeezing. Figure 4 shows the diffuse reflectance spectra of the $TTPH_2$ adsorbed on cation-exchanged MMT. The results are in good agreement with visible spectra, as all cation-exchanged MMT cause protonation of the $TTPH_2$ compound.

Figure 5 presents the visible absorption spectrum of $TNPH_2$ in glacial acetic acid on a Fe(III) MMT surface. Adsorption of $TNPH_2$ on Fe(III) MMT causes the Soret band to be shifted to an absorption wavelength higher than that of the free base. The shift of 15 nm when the compound is in the adsorbed state, and the behaviour of the compound in acetic acid, which showed only a small shoulder at a longer wavelength, help to understand how this porphyrin behaves when it's on the clay surface or possibly even in the interlayers.

Clearly, in the acetic acid, almost all the $TNPH_2$ molecules are not protonated. In and on the clay, the surfaces are much more like a strong acid and a large proportion of the $TNPH_2$ molecules are present as the dication, although there is evidence that some of the molecules are still present in the neutral form from the width of the Soret band and the presence of the four weak bands between 500 nm and 700 nm. It can be inferred that because the porphyrin molecule is a non-rigid aromatic system, the planar conformation is favorably affected by both the acidic character of the clay and the van der Waals and H bonds to the clay, hence the dication forms.

The diffuse reflectance spectrum of the $TNPH_2$ adsorbed on Fe(III) MMT sample also shows a shift in the Soret band (Figure 6).

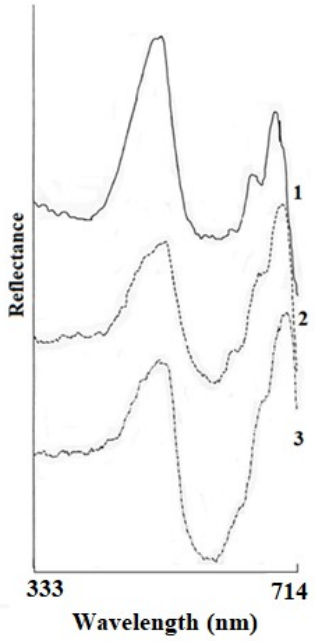

Figure 4: Diffuse reflectance spectra of $TTPH_2$ compound adsorbed on (1) Ni(II) MMT, (2) Fe (III) MMT, (3) Cd(II) MMT.

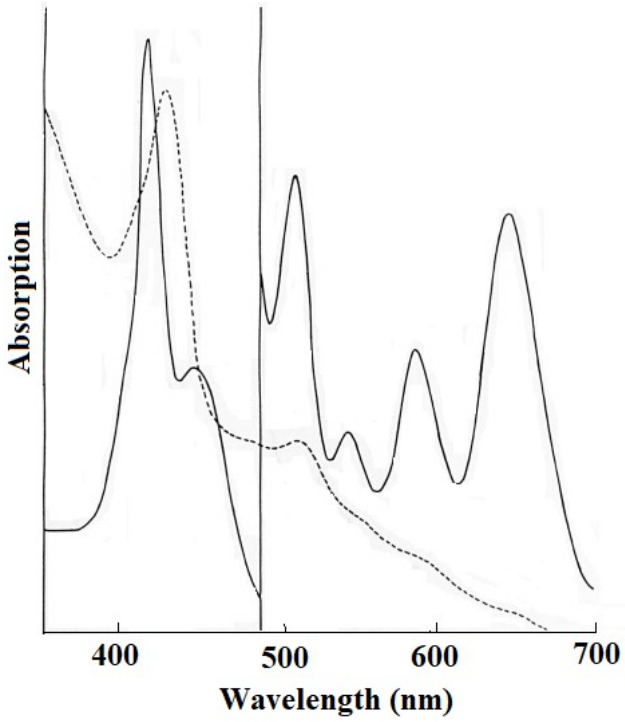

Figure 5: Visible absorption spectra of (_____) $TNPH_2$ in glacial acetic acid, (------) $TNPH_2$ on Fe(III) MMT. For clarity, the y-axis in the region from 500 nm to 700 nm has been magnified by 20 times for the visible absorption spectrum of $TNPH_2$ in acetic acid.

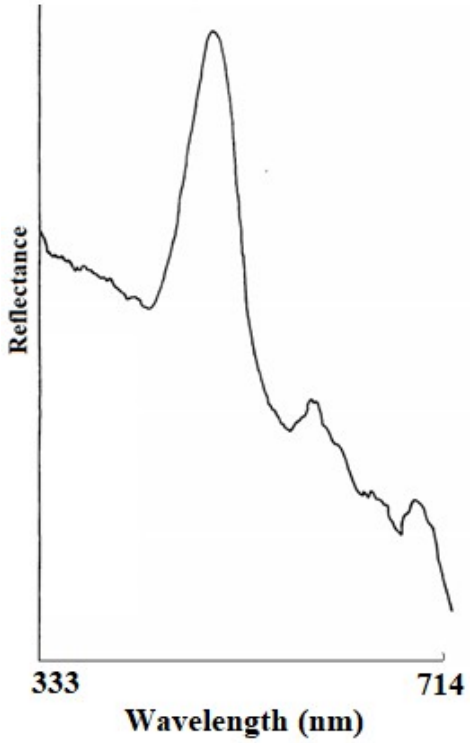

Figure 6: Diffuse reflectance spectrum of $TNPH_2$ compound adsorbed on Fe(III) MMT.

When the two compounds react with MMT saturated with metal ions of a suitable size to fit in the porphyrin ring, such as Cu(II), in a solvent miscible with water that facilitates the penetration of the hydrated sphere of the metal ion, the metal ions are incorporated into the porphyrin rings. This generates metalloporphyrin complexes. Figure 7 shows the visible absorption spectra of the two porphyrin compounds adsorbed onto Cu(II) MMT in acetone, clearly the Soret bands are around 420 nm, with three further bands between 530 nm and 600 nm. The spectra are similar to those reported for a Cu (II) porphyrin complex formed in solution (29) and are typical of porphyrins containing metals (note the absence of the four bands (between 500 nm and 700 nm) found in the unmetallated compounds.

The metal porphyrins formed on the MMT surface tend to be desorbed into the solution. These neutral complexes appear easily displaced from the exchange sites, presumably by the protons expelled from the porphyrin molecule during metallation.

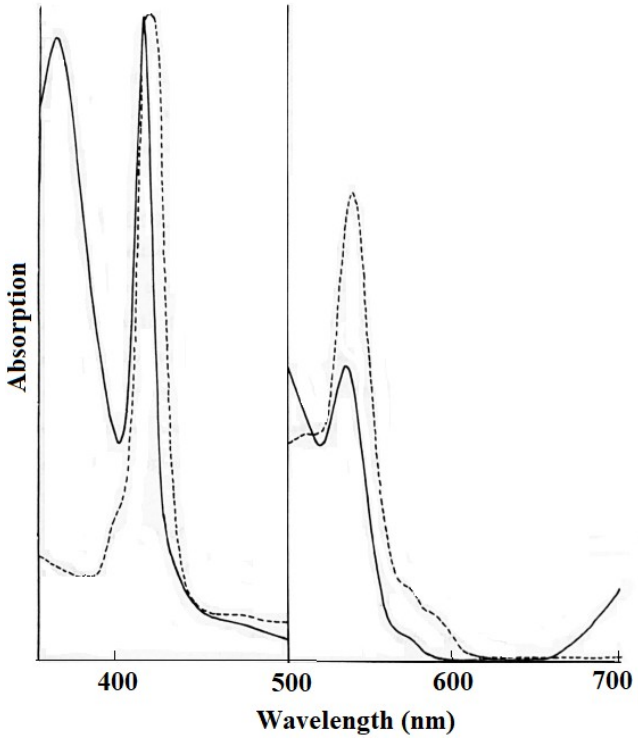

Figure 7: Visible absorption spectra of (_____) $TTPH_2$ and (------) $TNPH_2$ on Cu(II) MMT. For clarity, the y-axis in the region from 500 nm to 700 nm has been magnified by 20 times.

3.3. X-ray Powder Diffraction

The MMT gives a basal spacing of 9.6 Å, when there are no molecules between the unit layers and 13 Å if there are water molecules (30). When Cu(II) MMT was reacted with $TTPH_2$ in a solvent miscible with water like acetone, the sample gave basal spacing of 14 Å, indicating a 4.4 Å interlayer separation, due to the intercalation of the porphyrin complex that formed. The 4.4 Å is lower than expected, as the molecule thickness is 4.7 Å (31) (Figure 8). Others (7) have also observed a basal spacing for MMT when it reacted with $TPyPH_2$, lower than expected from the molecular geometry. They attributed this to a twisting of the molecule in the MMT interlayer. This fact is supported herein by the higher shifts in the visible spectra found when the molecules are in the adsorbed state rather than in an acetic acid solution.

The $TNPH_2$ compound did not show a separation of the layers, probably because the naphthalene entity has difficulty lying in the same plane as the porphyrin plane (possibly due to steric constraints on ring rotation). Thus, $TNPH_2$ has a greater width than $TTPH_2$, and in this case it needs more space to enter the interlayer without special treatment. All other samples didn't show any interlayer separation.

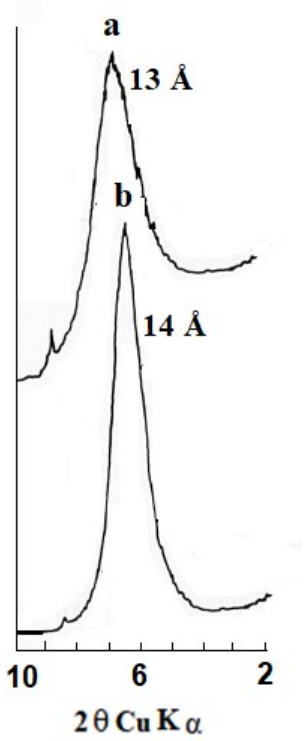

Figure 8: X-ray powder diffraction patterns of MMT (a) original sample, (b) Cu(II) MMT reacted with $TTPH_2$.

3.4. Electron Microscopy

The minerals of the MMT group are the most difficult clay minerals to be characterized by their morphology. To obtain adequate information about the samples, a high-resolution mode of operation was used. The MMT appeared as fibers under the electron microscope. The transmission electron micrograph of the Cu(II) MMT sample, which was reacted with $TTPH_2$ in acetone and had a basal spacing of 14 Å, is shown in Figure 9. The interlayer separation was 4.4 Å, which was attributable to porphyrin complex layering between the MMT interlayers. A group of striated black lines stacked between the MMT fabric may be seen in the micrograph. The porphyrin complex in the MMT interlayers is probably responsible for the dark lines.

Figure 9: Transmission electron micrographs of (left) MMT Sample, (right) Cu(II) MMT sample reacted with $TTPH_2$ in acetone.

4. CONCLUSION

When the two porphyrin compounds $TTPH_2$ and $TNPH_2$ react with MMT clay saturated with various cations, the former compound tends to be more planar in the MMT interlamellar and on the surface. If the metal ions on MMT, are of the suitable size to fit in the porphyrin ring such as Cu(II), a metal-porphyrin complex is formed (evidence presented herein). The later process takes place if the reaction is carried out in a solvent miscible with water like acetone, to penetrate the hydrated sphere of the metal ion. This type of complex has been formed in the reaction between Cu(II) MMT and both the porphyrins studied in this work. It has also been shown herein that larger porphyrins where the *meso* substituent is less free to rotate (here, $TNPH_2$) cannot penetrate the interlamellar spacings of the clays.

5. REFERENCES

1. Kosiur DR. Porphyrin Adsorption by Clay Minerals. Clays Clay Miner. 1977 Oct;25:365-71. Available from: <URL>.

2. Canesson P, Cruz MI, Van Damme H. X.P.S. study of the interaction of some porphyrins and metalloporphyrins with montmorillonite. Dev Sedimentol. 1979; 27; 217-25. Available from: <URL>.

3. Hassen JH. Spectroscopic analysis of adsorbed macrocyclic complexes on ceramic and related materials [PhD. Thesis]. [Colchester, England]: University of Essex; 1988.

4. Dias PM, de Faria DL, Constantino VR. Clay-porphyrin systems: Spectroscopic evidence of TMPyP protonation, non-planar distortion and *meso* substituent rotation. Clays Clay Miner. 2005 Aug; 53:361-71. Available from: <URL>.

5. Hassen J, Silver J. Stability of Fe(III) and Sn(IV) metalloporphyrins adsorbed on cation-exchanged montmorillonite. Trends Sci. 2022 Apr; 19(8):3426. Available from: <URL>.

6. Fujimura T, Shimada T, Hamatani S, Onodera S, Sasai R, Inoue H, et al. High density intercalation of porphyrin into transparent clay membrane without aggregation. Langmuir. 2013 Mar; 29(16):5060-65. Available from: <URL>.

7. Van Damme H, Crespin M, Obrecht F, Cruz MI, Fripiat JJ. Acid-base and complexation behavior of porphyrins on the intracrystal surface of swelling clays: *meso*-tetraphenylporphyrin and *meso*- tetra(4-pyridyl)porphyrin on montmorillonites. J Colloid Interface Sci. 1978 Aug;66(1):43-54. Available from: <URL>.

8. Nishina H, Hoshino S, Ohtani Y, Ishida T, Shimada T, Takagi S. Anisotropic energy transfer in a clay–porphyrin layered system with environment-responsiveness. Phys Chem Chem Phys. 2020 Jun;22(25):14261-67. Available from: <URL>.

9. Auwarter W, Ecija D, Klappenberger F, Barth JV. Porphyrins at interfaces. Nat Chem. 2015 Jan;7:105-20. Available from: <URL>.

10. Takagi S, Eguchi M, Tryk DA, Inoue H. Light-harvesting energy transfer and subsequent electron transfer of cationic porphyrin complexes on clay surfaces. Langmuir. 2006 Jan;22(4):1406-8. Available from: <URL>.

11. Ishida Y, Shimada T, Masui D, Tachibana H, Inoue H, Takagi S. Efficient excited energy transfer reaction in clay/porphyrin complex toward an artificial light-harvesting system. J Am Chem Soc. 2011 Aug;133(36):14280-86. Available from: <URL>.

12. Ishida Y, Masui D, Tachibana H, Inoue H, Shimada T, Takagi S. Controlling the microadsorption structure of porphyrin dye assembly on clay surfaces using the "size-matching rule" for constructing an efficient energy transfer system. ACS Appl Mater Interfaces. 2012 Jan; 4(2):811-16. Available from: <URL>.

13. Ishida Y, Shimada T, Tachibana H, Inoue H, Takagi S. Regulation of the collisional self-quenching of fluorescence in clay/porphyrin complex by strong host-guest interaction. J Phys Chem. A. 2012 Nov;116(49):12065-72. Available from: <URL>.

14. Egawa T, Watanabe H, Fujimura T, Ishida Y, Yamato M, Masui D, et al. Novel methodology to control the adsorption structure of cationic porphyrins on the clay surface using the "size-matching rule". Langmuir. 2011 Jul;27(17):10722-29. Available from: <URL>.

15. Takagi S, Eguchi M, Yui T, Inoue H. Photochemical Electron Transfer Reactions in Clay-porphyrin Complexes. Clay Sci. 2006; 12(2): 82-7. Available from: <URL>.

16. Takagi S, Konno S, Ishida Y, Ceklovsky A, Masui D, Shimada T, et al. A unique "Flattening effect" of clay on the photochemical properties of metalloporphyrins. Clay Sci. 2010; 14(6):235-39. Available from: <URL>.

17. Ishida Y, Fujimura, T, Masui D, Shimada T, Tachibana H, Inoue H, et al. What lowers the efficiency of an energy transfer reaction between porphyrin dyes on clay surface? Clay Sci. 2011; 15(4):169-74. Available from: <URL>.

18. Carrado KA, Wasserman SR. Stability of Cu(II)− and Fe(III)−porphyrins on montmorillonite clay: An x-ray absorption study. Chem. Mater. 1996 Jan;8(1):219-25. Available from: <URL>.

19. Bergaya F, Van Damme H. Stability of metalloporphyrins adsorbed on clays: A comparative study. Geochim Cosmochim Acta. 1982 Mar;46(3):349-60. Available from: <URL>.

20. Abdo S, Cruz MI, Fripiat JJ. Metallation-demetallation reaction of tin tetra(4-pyridyl) porphyrin in Na-hectorite. Clays Clay Miner. 1980 Apr; 28: 125-29. Available from: <URL>.

21. Crestini C, Pastorini A, Tagliatesta P, Metalloporphyrins immobilized on motmorillonite as biomimetic catalysts in the oxidation of lignin model compounds. J Mol Catal A Chem. 2004 Feb;208(1-2):195-202. Available from: <URL>.

22. Machado AM, Wypych F, Drechsel SM, Nakagaki S (2002) Study of the catalytic behavior of montmorillonite/iron (III) and Mn(III) cationic porphyrins. J Colloid Interface Sci. 2002 Oct; 254:158–64. Available from: <URL>.

23. Zyoud A, Jondi W, Mansour W, Majeed Khan MA, Hilal HS. Modes of tetra(4-pyridyl)porphyrinatomanganese(III) ion intercalation inside natural clays. Chem Cent J. 2016 Mar;10:12. Available from: <URL>.

24. Hassen JH, Silver J. Stability of Fe(III) and Sn(IV) Metalloporphyrins Adsorbed on Cation-Exchanged Montmorillonite. Trends Sci. 2022 Mar;19(8):3426-34. Available from: <URL>.

25. Adler AD, Lengo FR, Finarelli JD, Goldmacher J, Assour J, Korsakoff L. A simplified synthesis for meso-tetraphenylporphine. J Org Chem. 1967 Feb; 32(2):476. Available from: <URL>.

26. Noskov AV, Alekseeva OV, Shibaeva VD, Agafonov AV. (2020). Synthesis, structure and thermal properties of montmorillonite/ionic liquid ionogels. RSC Adv. 2020 Sep; 10(57):34885- 94. Available from: <URL>.

27. Rozenson I, Heller-Kallai L. Reduction and oxidation of Fe^{3+} in dioctahedral smectites-III. Oxidation of octahedral iron in montmorillonite. Clays Clay Miner. 1978 Apr;26:88-92. Available from: <URL>.

28. Holtzer M, Bobrowski A, Grabowska B. Montmorillonite: A comparison of methods for its determination in foundry bentonites. Metalurgija. 2011 Apr; 50(2):119-22.

29. Jeong D, Kang D-g, Joo T, Kim SK. Femtosecond-resolved excited state relaxation dynamics of copper (II) tetraphenylporphyrin (CuTPP) after soret band excitation. Sci Rep. 2017 Des;7:16865. Available from: <URL>.

30. Hassen J, Silver J. Montmorillonite surface as a catalyst for the formation of SAT metal tetra(*p*-sulphophenyl)porphyrins. J Teknol. 2020 Nov;82(6):1-9. Available from: <URL>.

31. Falk JE. Porphyrins and metalloporphyrins. Amsterdam; Elsevier; 1964. 266 p. Available from: <URL>.